Bioorganic Chemistry 105 (2020) 104390

Contents lists available at ScienceDirect

Bioorganic Chemistry

journal homepage: www.elsevier.com/locate/bioorg

Discovery of novel sulfonamide-containing aminophosphonate derivatives as selective COX-2 inhibitors and anti-tumor candidates

Bo Zhang [a], Xiu-Ting Hu [a], Jin Gu [a], Yu-Shun Yang [a,*], Yong-Tao Duan [b,*], Hai-Liang Zhu [a,*]

[a] State Key Laboratory of Pharmaceutical Biotechnology, Nanjing University, Nanjing 210023, PR China
[b] Henan Provincial Key Laboratory of Children's Genetics and Metabolic Diseases, Children's Hospital Affiliated to Zhengzhou University, Zhengzhou University, Zhengzhou 450018, PR China

ARTICLE INFO

Keywords:
Cyclooxygenase-2
Anti-tumor
Sulfonamide moiety
Aminophosphonate derivatives
Apoptosis induction
Mitochondrion-dependent mode

ABSTRACT

As an essential enzyme with a variety of physiological functions, Cyclooxygenase-2 (COX-2) is also closely related to carcinoma due to the observed overexpression. In this work, a novel series of sulfonamide-containing aminophosphonate derivatives (**A1-A25**) were developed as selective COX-2 inhibitors and anti-cancer candidates. The top hit compound **A23** presented applicative COX-2 inhibitory activity (IC_{50} = 0.28 μM) and anti-proliferative capability against several cancer cell lines (IC_{50} = 2.34–16.43 μM for HeLa, MCF-7, HCT116 and HepG2 cells). Among them, A23 has the most significant inhibitory effect on HCT116 cells, which were comparable with that of the positive controls respectively (eg: IC_{50} = 8.73 μM for HCT116). The binding pattern of **A23** was inferred by the molecular docking simulation. Moreover, **A23** could induce the apoptosis via a mitochondrion-dependent mode and cause the arrest of the cell-cycle in G1 stage. A further investigation in the checkpoints of apoptosis indicated that the node Bcl-2 might connect the selective COX-2 inhibition and the anti-tumor activity. Therefore, this work brought new information for developing COX-2 inhibitors in anti-tumor therapies in future.

1. Introduction

Prostaglandin (PGs), a vital series of aliphatic acids, play significant role in the physiological and pathological processes including platelet aggregation, cardiovascular balance, inflammation and tumor progression. Cyclooxygenase (COX), transforming arachidonic acid into PGs, is the rate-limiting enzyme of the biosynthesis of PGs [1–3]. There exist at least two isoenzymes of COX. One is COX-1, the structural protein found in blood vessels, stomach and kidney, thus functioning in the vasoconstriction, gastric mucosal injury and renal regulation, respectively [4]. The other is COX-2, the inducible enzyme anchored in the nuclear membrane, showing an obvious overexpression during the pathological events [5]. It has been known for a long time that the expression of COX-2 is up-regulated significantly after the occurrence of inflammation [6]. Recently, the interest of the investigators on COX-2 has been drawn to its overexpression in a variety of tumors such as breast cancer and pancreatic cancers [7]. The level of COX-1 indicated no obvious variation in these cancer models [8]. Thus selectively inhibiting COX-2 seems a favorable strategy for designing therapeutic methods for carcinomas. Since a large number of COX-2 inhibitors have been discovered as non-steroidal anti-inflammatory drugs (NSAIDs) [9], there have been a plenty sample size to check their performances in the anti-proliferation, apoptosis induction and metastasis prevention [10]. Therefore, seeking the connection between COX-2 inhibition and anti-tumor activity has become an interesting research topic [11].

Glancing at the numbers of references each year in Web of Science during the period of 2000–2020 (Fig. 1), we could conclude that COX-2 was a hotspot in this field and approximate 30% of the reports were associated with cancers. Many factors or nodes in the pathways, such as PTEN [12], PI3K/Akt/mTOR/S6K1 [13], MAPK [14], NF-κB [15], TNF-α [16], CDK [17] and Bcl-2 [18], were involved to draw the mechanism of COX-2 inhibitors for anti-tumor applications. However, till now, no clear map was depicted due to several problems including the target-missing caused by nonspecific structure, the complex inflammation-tumor interactions, and the sophisticated environmental factors. As a solution strategy, we attempted to explore the potential mechanism with selective inhibitors, key checkpoints and simplified indicators.

In this work, we designed the novel compounds on the structural basis of known COX-2 inhibitors such as Celecoxib [19] and Valdecoxib [20] (shown in Fig. 2). The five-membered nitrogen heterocyclic core

* Corresponding authors.
E-mail addresses: ys_yang@nju.edu.cn (Y.-S. Yang), duanyongtao860409@163.com (Y.-T. Duan), zhuhl@nju.edu.cn (H.-L. Zhu).

https://doi.org/10.1016/j.bioorg.2020.104390
Received 23 July 2020; Received in revised form 4 October 2020; Accepted 15 October 2020
Available online 20 October 2020

and sulfonamide moiety were both retained to maintain the basic COX-2 inhibition and selectivity according to the reports [21,22]. The other fragment we introduced, the aminophosphonate group, was recently investigated in enhancing both the anti-tumor and anti-inflammation effects [23–28]. The designed compounds were preliminarily checked by virtual screening of ADMET and molecular docking simulation. The prepared series was then evaluated according to their performance on COX-2 and several cancer cells lines. After confirming the mitochondrion-dependent apoptosis induction and cell-cycle arrest, further investigation in the checkpoints was conducted to infer the connection between the selective COX-2 inhibition and the anti-tumor activity by this series.

2. Results and discussion

2.1. Chemistry

The chemical synthesis route to compounds **4a-4k** are outlined in Scheme 1. First, the substituted acetophenones were reacted with dimethyl oxalate in sodium methoxide-methanol solution to produce the intermediates **2a-2k**. Then the intermediate **3a-3k** were obtained through the reaction of **2a-2k** with 4-hydrazinylbenzenesulfonamide. Finally, these pyrazole methyl ester **3a-3k** was hydrolyzed by sodium hydroxide into the corresponding acids **4a-4k**. The synthesis of compounds **A1-A25** was described in Schemes 2. The corresponding acids **4a-4k** was activated with EDC·HCl, DMAP and HOBt at 0 °C for 30 min, then reacted with different aminophosphonate derivatives to produce the target compounds **A1-A25** through amide condensation reaction. Aminophosphonate derivatives were synthesized according to the literature [29]. The solvent used in the above steps was anhydrous dichloromethane. The target compounds **A1-A25** were purified by column chromatography and their structures were shown in Table 1. Compounds **A1-A25** were reported for the first time and characterized by ^{1}H NMR spectra, ^{1}C NMR spectra, melting point and ESI-MS, in accordance with their depicted structures.

2.2. COX-2 inhibitory activities and selectivity

The initial task of this work was the evaluation of the selective COX-2 inhibition of the synthesized compounds. By using the human COX-1/COX-2 ELSIA kit, we obtained the required data including both the inhibitory activities of COX-2 and COX-1. As shown in Table 2, all this series indicated potent inhibition upon COX-2 and a majority of them suggested obvious selectivity from COX-1. Among them, the most attractive compound, **A23**, showed a comparable COX-2 inhibitory activity with the positive control Celecoxib and **A33** in another study, Zhu *et al.* [30] (IC_{50} values: 0.28 μM vs. 0.24 μM and 0.17 μM) but a significantly better selectivity (Selectivity Index: 172.32 vs. 93.25). A glance at the substitutes led to some hints about the Structure-Activity Relationship (SAR). For COX-1 inhibition, the IC_{50} values of all this series were in a narrow range (25.63–51.62 μM, almost within 2-fold). Cheerfully, in this aspect, these series showed less potency than Celecoxib, which conversely contributed to the selectivity towards COX-2. With close COX-1 inhibition, better performance against COX-2 meant better selectivity as well. In the case of electron-withdrawing groups at R^1 (-F, -Cl, -CF_3), R^2 substitutes seemed to prefer a smaller size, with the corresponding examples (“>” meant “better than”): **A1** > **A2**, **A3** > **A4**, **A7** > **A8**, **A9** > **A10**, **A11** > **A12**, **A16** > **A17**. The only exception was **A5** and **A6** with the *othro*-fluoro group, being strong electron-withdrawing and close to the pyrazole core. On the contrary, in the case of electron-donating groups at R^1 (-Br(*para*), -Me, -OMe), R^2 substitutes seemed to prefer a bulky size, with the corresponding examples: **A15** > **A14**, **A20** > **A19**, **A22** > **A21**, **A25** > **A24**. Fortunately, we involved methyl at R^2, which brought fluctuation to cause more favorable (**A18**, **A23**) or unfavorable (**A13**) results. Although the difficult in synthesis increased at this site, an aliphatic group and a corresponding discussion seemed an interesting point in the near future.

2.3. Molecular docking simulation

To visualize the possible binding pattern of the hit compound **A23** into COX-2, the molecular docking simulation was performed with the Protein Crystal Structure of COX-2 bearing Celecoxib (PDB code: 3LN1). The obtained maps were depicted in Fig. 2. As shown in Fig. 3A and the detailed Fig. 3B, the general extension directions were similar between **A23** and Celecoxib, which might explain their close potency. However, longer substitutes of **A23** seemed to bring more potential interactions with the key residues in COX-2, while at the same time avoid the off-target effect which was usually caused by the small molecular size. When we compared the possible interactions in detail with Fig. 3C and D, we found that **A23** included more interactions with more residues. Although COX-2 seemed a typical case which agreed with the Lipinski’s “Rule of Five” in hydrogen bonds, its interactions relied seriously on the sulfonamide and electron-withdrawing trifluoromethyl. However, as we discussed in the preliminary SAR after the COX-2 inhibition, in the case of **A23**, when retaining the important sulfonamide, an electron-donating group allowed the backbone to extend further. Afterwards the substitutes around the pyrazole core were redistributed, which led to the key interactions with almost all the rings and chains of **A23**. Based on the fact that the COX-2 inhibition ability of **A23** and Celecoxib, we supposed that a better selectivity and less off-target effect might resulted in better potency on cancer cells.

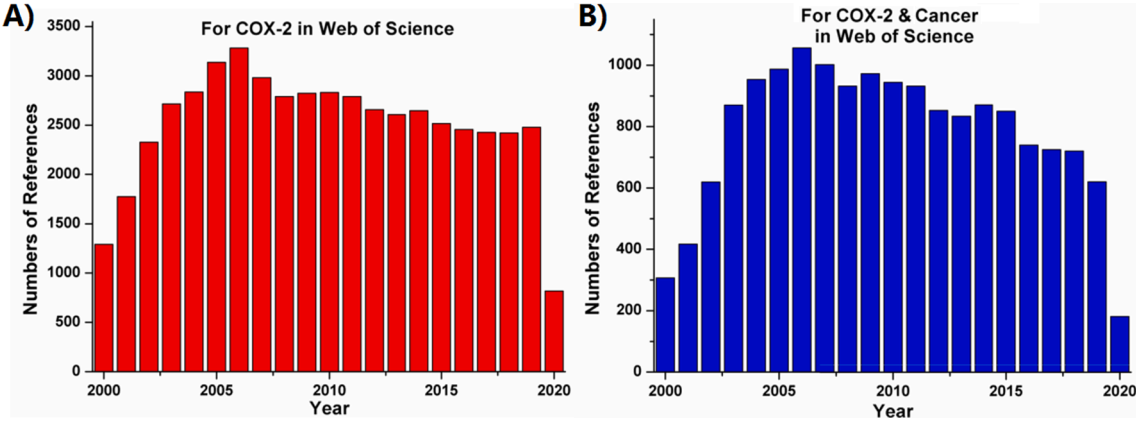

Fig. 1. The numbers of references each year in Web of Science during the preriod of 2000–2020 for COX-2 only and COX-2 with cancers. (Searching keywords: COX-2, Cancer; Searching date: 2020.07.15).

2.4. Anti-proliferation assay

The anti-proliferative activities of all compounds against four tumor cell lines (HeLa, human cervical cancer cells; MCF-7, human breast cancer cells; HCT116, human colon cancer cells; HepG2, human liver cancer cells) was determined by employing MTT method. Besides, the cytotoxicity was checked by the epithelial cell line 293T. As shown in Table 3, a majority of these series indicated potent anti-proliferative activity against all the investigated cancer cells and low toxicity upon the epithelial cells. Since the pathway from COX-2 down to tumor is not clear, there might be complex factors all through the whole process. Therefore, no rigid one-to-one correspondence could be generated between the COX-2 inhibition and the anti-tumor effect. But still, we found that the top hits in COX-2 inhibitory assay (**A3**, **A7**, **A9**, **A11**, **A23**, **A25**) also showed better potency against the growth of the cancer cells. As the chosen hit above, **A23** seemed potential for cancer treatment (IC_{50} values: 9.71 μM for HeLa, 16.43 μM for MCF-7, 2.34 μM for HCT116, 12.51 μM for HepG2). This result is much better than that of Celecoxib (**(**IC_{50} values: 25.72 μM**)** and **7m** (IC_{50} values: 8.07 μM) in in another study, Wang *et al.* [31], being comparable with the anti-cancer drug Cisplatin. Thus, **A23** was further studied in the subsequent experiments with the most affected HCT116 cells.

2.5. Cell apoptosis, cell cycle arrest and mitochondrial membrane potential.

The COX-2-related anti-tumor effect was reported to be associated with the induction of cell apoptosis. As shown in Fig. 4, along with the increase of **A23** concentration (0, 5, 10 and 20 μM), the 48 h-incubated cells also exhibited an increased percentage of apoptotic cells (9.22%, 20.5%, 23.4%, 42.5%). This result inferred that **A23** could induce cell apoptosis in a dose-dependent manner. Besides, the proportion of early apoptosis cells was equal to that of late apoptosis ones.

Since cell cycle arrest was another reported phenomenon through the COX-2-related anti-tumor cases, we also studied this factor by using propidium iodide (PI) staining. With the same time and concentration conditions, a cell cycle arrest at G1 phase was observed. As shown in Fig. 5, with the increased concentration of **A23**, the percentage of cells arrested in G1 phase exhibited a corresponding increase (58.77%, 67.24%, 72.44%, 79.96%). Therefore, in a dose-dependent manner, **A23** could block cell mitosis at G1 phase. This result was different from a commonly reported G2/M phase arrest, inferring that our series might experience less off-target effect.

Mitochondrial membrane potential decrease is the earliest change in cell apoptosis. Herein the apoptosis-inducing effect of **A23** on HCT116 cells were determined by JC-1 assay. HCT116 cells were treated with compound **A23** (0, 2.5, 5, 10, and 20 μM) for 24 h and stained with JC-1. As shown in Fig. 6, along with the concentration increased from 2.5 μM to 20 μM, the fluorescence of cells gradually changed from red to green. The results indicated that **A23** could induce the apoptosis of HCT116 cells in a dose-dependent manner.

2.6. Investigations on the apoptosis checkpoints

The above results attributed the anti-tumor effect to cell cycle arrest. Herein we studied the apoptosis checkpoints to hint the connection between the selective COX-2 inhibition and the anti-tumor activity. The involved checkpoints included c-parp, Bcl-2, BAX, and Caspase 3, 4, 6, 7, 8, 9. The results in Fig. 7 indicated that the apoptosis event caused by our series was correlated to almost all the checkpoints except for Caspase 4 and 8. At least we could conclude at this step that the apoptosis was through a mitochondrion-dependent mode. Afterwards, we attempted to track back the upstream node. As the key point of PI3K/Akt/mTOR/S6K1 and MAPK pathways, Akt and ERK were checked (Fig. S1 in Supporting Information). Surprisingly, both of the checked points were affected when COX-2 was inhibited. This result indicated that in the anti-cancer events, COX-2 might be in the upper position of both the pathways, while the unbalanced transduction in these pathways converge at Bcl-2. Therefore, we could preliminarily infer that Bcl-2 might be regulated by COX-2 with a following induction of apoptosis. In the near future, we would seek the key nodes between Bcl-2 and COX-2 with a more detailed interaction net.

3. Conclusion

In this work, a novel series of sulfonamide-containing aminophosphonate derivatives were developed as selective COX-2 (the mediator of cell survival, proliferation and apoptosis) inhibitors and anticancer candidates. Via evaluating both the COX-2 inhibition and selectivity, we chose **A23** as the top hit, which exhibited applicative COX-2

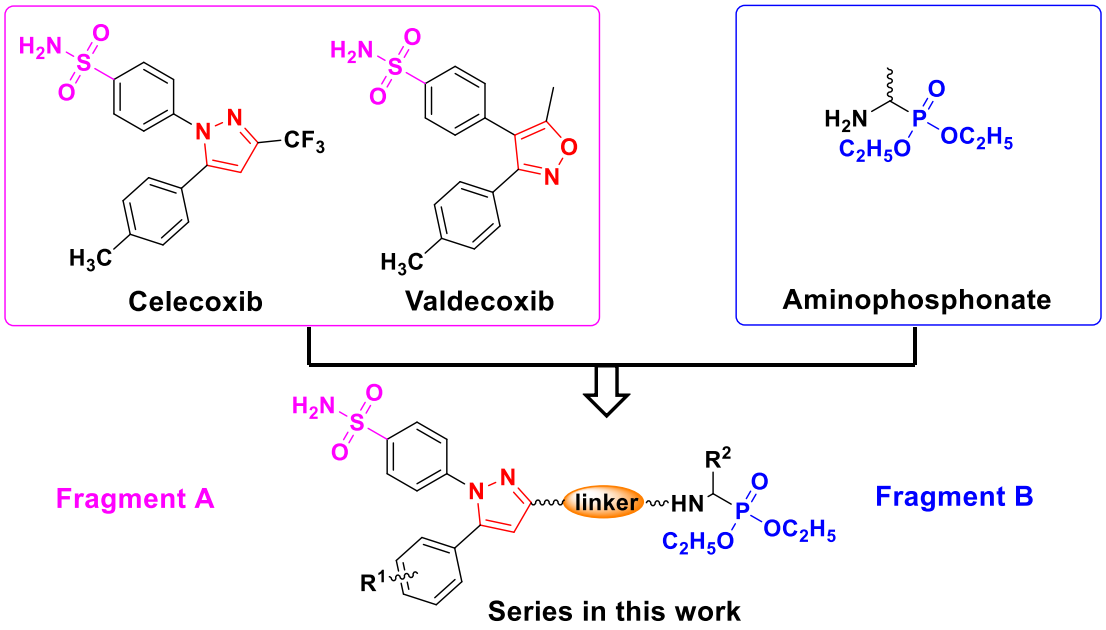

Fig. 2. The designing concept of the series in this work as selective COX-2 inhibitors.

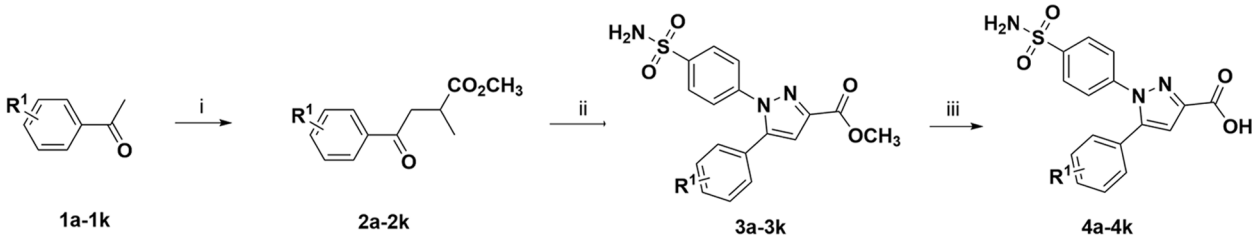

Scheme 1. Reagents and conditions: (i) Dimethyl oxalate, Sodium methoxide, MeOH, reflux, 12 h, ice water, dilute hydrochloric acid; (ii) 4-hydrazinobenzenesulfonamide hydrochloride, MeOH, 70 °C, 4–6 h; (iii) NaOH, MeOH, 70 °C, 4 h.

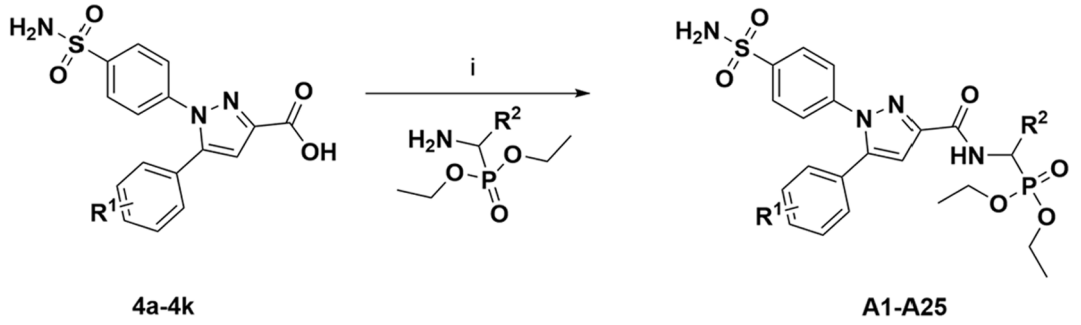

Scheme 2. Reagents and conditions: (i), EDC·HCl, DMAP, HOBt, CH_2Cl_2, r.t, overnight.

Table 1

Structures of compounds **A1-A25**.

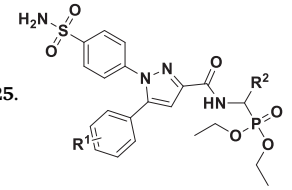

Code	R^1	R^2	Code	R^1	R^2
A1	4-Fluoro	Phenyl	**A14**	4-Bromo	Phenyl
A2	4-Fluoro	4-Bromophenyl	**A15**	4-Bromo	4-Bromophenyl
A3	3-Fluoro	Phenyl	**A16**	4-Trifluoromethyl	Phenyl
A4	3-Fluoro	4-Bromophenyl	**A17**	4-Trifluoromethyl	4-Bromophenyl
A5	2-Fluoro	Phenyl	**A18**	4-Methyl	Methyl
A6	2-Fluoro	4-Bromophenyl	**A19**	4-Methyl	Phenyl
A7	4-Chloro	Phenyl	**A20**	4-Methyl	4-Bromophenyl
A8	4-Chloro	4-Bromophenyl	**A21**	4-Methoxy	Phenyl
A9	3-Chloro	Phenyl	**A22**	4-Methoxy	4-Bromophenyl
A10	3-Chloro	4-Bromophenyl	**A23**	3-Methoxy	Methyl
A11	2-Chloro	Phenyl	**A24**	3-Methoxy	Phenyl
A12	2-Chloro	4-Bromophenyl	**A25**	3-Methoxy	4-Bromophenyl
A13	4-Bromo	Methyl			

Table 2

COX-1/COX-2 inhibitory activity of compounds **A1-A25** and Celecoxib.

Compounds	IC_{50} ± SD (μM)[a]		Selectivity Index[b] (SI)
	COX-1	COX-2	
A1	45.74 ± 1.25	1.19 ± 0.18	38.44
A2	39.65 ± 2.01	1.21 ± 0.26	32.77
A3	32.05 ± 0.92	0.27 ± 0.02	118.70
A4	45.26 ± 0.45	3.94 ± 0.21	11.49
A5	44.08 ± 1.08	4.63 ± 0.52	9.52
A6	41.25 ± 1.31	3.17 ± 0.13	13.01
A7	27.63 ± 1.82	0.31 ± 0.08	89.13
A8	45.36 ± 0.91	6.32 ± 1.37	7.18
A9	32.17 ± 0.38	0.28 ± 0.03	114.89
A10	38.76 ± 1.36	0.45 ± 0.14	86.13
A11	36.24 ± 0.85	0.33 ± 0.11	109.82
A12	42.18 ± 1.09	2.19 ± 0.24	19.26
A13	35.92 ± 0.23	3.96 ± 0.62	9.07
A14	35.86 ± 1.59	2.37 ± 0.35	15.13
A15	48.51 ± 2.14	0.53 ± 0.04	91.53
A16	38.24 ± 1.61	2.74 ± 1.57	13.96
A17	30.73 ± 0.78	5.68 ± 0.82	5.41
A18	47.14 ± 1.19	0.95 ± 0.35	49.62
A19	41.21 ± 0.54	5.16 ± 0.26	7.99
A20	46.43 ± 1.05	1.28 ± 0.15	36.27
A21	51.62 ± 0.71	1.27 ± 0.29	40.65
A22	25.63 ± 1.26	0.45 ± 0.07	56.96
A23	48.25 ± 1.93	0.28 ± 0.05	172.32
A24	35.19 ± 1.47	0.54 ± 0.16	65.16
A25	29.55 ± 0.39	0.35 ± 0.03	84.43
Celecoxib	22.38 ± 0.65	0.24 ± 0.09	93.25

[a] The concentration of test compound required to produce 50% inhibition of COX-1/COX-2 is the mean of four determinations.

[b] *In vitro* COX-2 selectivity index (COX-2 IC_{50}/COX-1 IC_{50}).

inhibitory activity (IC_{50} = 0.28 ± 0.05 μM) and anti-proliferative capability against several cancer cell lines. The selectivity of **A23** towards COX-2 (Selectivity Index 172.32) was much better than the control Celecoxib. Molecular docking simulation hinted that this kind of potency and selectivity might be related to the binding interactions with the key residues including Val102, Arg106, Val335, Tyr371, Arg499, Ala513 and so on. The anti-proliferation effect was inferred to be led through an apoptosis induction via a mitochondrion-dependent mode with the cell cycle arrest at G1 stage. After investigating the checkpoints of apoptosis, we preliminarily deduced that the node Bcl-2 might connect the selective COX-2 inhibition and the anti-tumor activity. Although more elaborate mechanism from COX-2 to Bcl-2 seems still difficult for us to reveal with a single study, we will try our best to depict

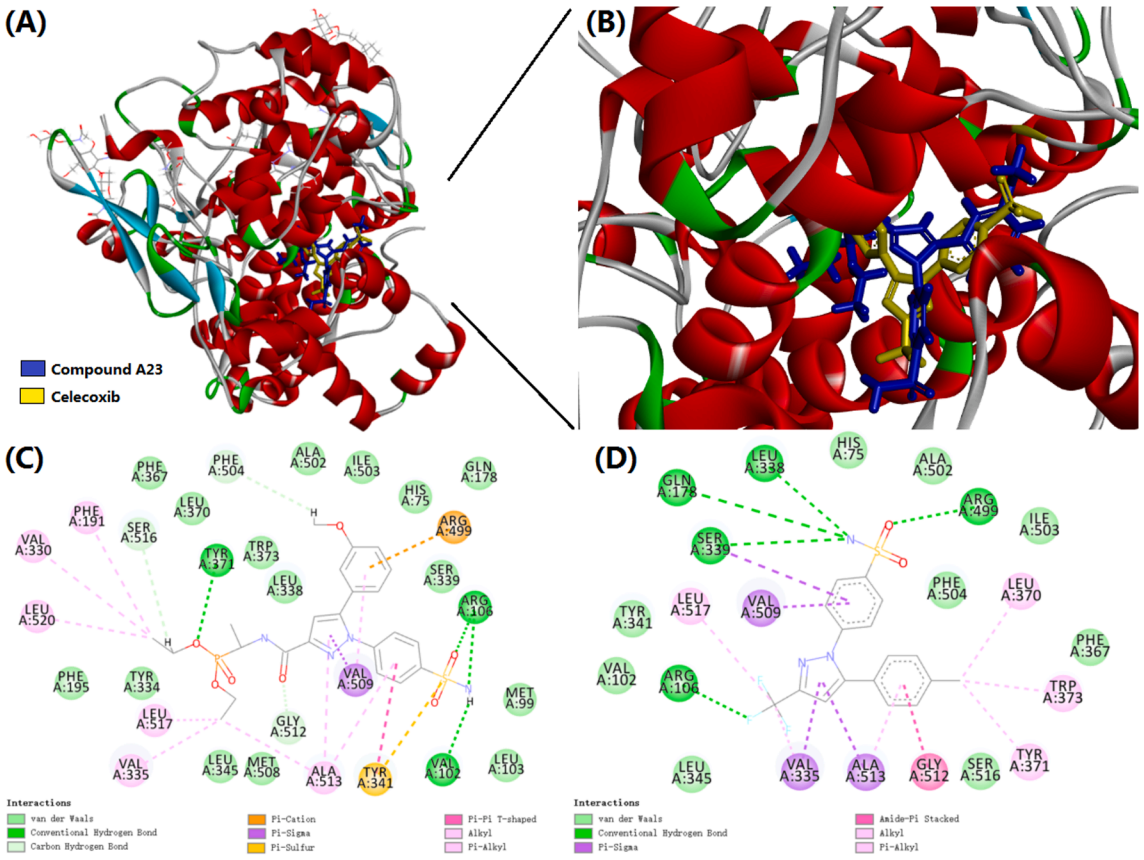

Fig. 3. The binding patterns of hit compound **A23** and Celecoxib into the active site of COX-2 (PDB code: 3LN1). (A) 3D binding map showing the site; (B) Detailed conformations in the binding site; (C) 2D binding pattern of **A23** into COX-2; (D) 2D binding pattern of Celecoxib into COX-2.

the panorama of this map for developing COX-2 inhibitors in anti-tumor therapies in future.

4. Experimental section

4.1. Materials and measurements

All chemical reagents and solvents purchased from Aladdin (China) were of analytical grade. All the melting points were determined with an X4 MP apparatus. NMR spectra were recorded in CDCl3 and $DMSOd_6$ on a Bruker DPX600 model spectrometer. A series of cell function experiments were analyzed by flow cytometry (BD FACSCalibur Flow Cytometry) and Fluorescence microscope (OLYMPUS IX71). The PCR amplification was evaluated on a LightCycler ® 480 II System (Roche). All cells were purchased from American type culture collection and conserved at State Key Laboratory of Pharmaceutical Biotechnology, Nanjing University, Nanjing. Cells were used in experiments after 3 times of passages.

4.2. General procedure for compounds *2a-2k*

Different substituted acetophenones (1 mmol) were added to anhydrous methanol, followed by dimethyl oxalate (2 mmol) and sodium methoxide (2 mmol). The above mixture was stirred at reflux for 12 h. After cooling to room temperature, the mixture solution was poured into ice water (150 mL) and treated with dilute hydrochloric acid (1 mol/L) to pH = 4. The precipitate was filtered, washed and dried in vacuo [32].

4.3. General procedure for compounds *3a-3k*

A mixture of 4-hydrazinylbenzenesulfonamide (2 mmol) and compounds **2a-2k** (1 mmol) in anhydrous methanol (20 mL) was stirred at reflux for 6 h. After confirming completion of the reaction, the reaction mixture was poured into water. The solid compounds **3a-3k** were isolated by filtration.

4.4. General procedure for compounds *4a-4k*

Sodium hydroxide (4 mmol) and compounds **3a-3k** (1 mmol) were added in anhydrous methanol and heated at reflux for 6 h. Then the reaction mixture was acidified with the hydrochloric acid solution (1 mol/L) and extracted with ethyl acetate (3 × 100 mL). The combined organic layer was dried over anhydrous sodium sulfate and concentrated in vacuo to obtain compound **4a-4k**.

4.5. General procedure for compounds *A1-A25*

EDC (1.2 mmol), HOBT (1.2 mmol) and DMAP (0.5 mmol) were added to a solution of 4a-4 k (1 mmol) in anhydrous dichloromethane. After stirring at 0 °C for 30 min, a-aminophosphonate (2 mmol) was added to the mixture and stirred for 5 h at room temperature. The crude product was purified by column chromatography with ethyl acetate and petroleum ether (V: V = 1:1) to give the final product **A1-A25**.

4.5.1. Diethyl((5-(4-fluorophenyl)-1-(4-sulfamoylphenyl)-1H-pyrazole-3-carboxamido)(phenyl)methyl)phosphonate (*A1*)

Yellow solid, yield 71.2%, m.p.: 87.6–88.2 °C. ^{1}H NMR (600 MHz, DMSO-d_6) δ 8.71 (dd, J = 9.8, 3.5 Hz, 1H), 7.91 (d, J = 8.6 Hz, 3H), 7.68 (d, J = 8.3 Hz, 1H), 7.60 (d, J = 8.6 Hz, 3H), 7.54 (s, 2H), 7.40–7.36 (m, 4H), 7.28 (t, J = 8.8 Hz, 2H), 7.17 (s, 1H), 5.70 (dd, J = 21.7, 9.8 Hz, 1H), 4.08 (d, J = 7.2 Hz, 2H), 3.98–3.94 (m, 1H), 3.85 (dd, J = 17.9, 7.9 Hz, 1H), 1.21 (t, J = 7.0 Hz, 3H), 1.10 (t, J = 7.0 Hz, 3H). ESI-MS: 587.15

Table 3
Anti-proliferative activities of compounds **A1-A25**, Celecoxib and Cisplatin.

Code	IC_{50} ± SD (μM)[a]				
	HeLa	MCF-7	HCT116	HepG2	293 T
A1	13.81 ± 1.57	10.12 ± 1.65	16.51 ± 1.28	10.53 ± 0.42	117.75 ± 1.34
A2	19.02 ± 1.36	23.04 ± 0.37	21.38 ± 0.26	16.34 ± 0.81	206.48 ± 1.01
A3	11.08 ± 0.04	5.32 ± 0.65	10.45 ± 1.03	8.73 ± 1.26	83.17 ± 3.12
A4	13.27 ± 0.96	18.07 ± 0.49	16.43 ± 0.52	17.28 ± 0.74	104.56 ± 1.51
A5	21.74 ± 0.78	15.76 ± 1.37	16.12 ± 0.39	21.17 ± 1.09	185.87 ± 0.63
A6	28.58 ± 0.31	26.83 ± 0.18	20.46 ± 0.57	28.16 ± 0.95	125.49 ± 1.14
A7	7.25 ± 0.23	>100	18.04 ± 1.41	7.64 ± 0.82	106.02 ± 1.42
A8	20.19 ± 0.61	28.09 ± 1.38	>100	16.71 ± 1.04	>300
A9	18.38 ± 1.92	6.39 ± 0.15	11.93 ± 0.36	>100	157.36 ± 0.97
A10	21.44 ± 0.85	12.47 ± 0.68	13.20 ± 1.03	15.78 ± 0.72	>300
A11	14.52 ± 1.34	16.94 ± 0.25	16.58 ± 0.43	13.96 ± 0.26	114.23 ± 1.81
A12	35.28 ± 0.19	20.91 ± 0.57	34.87 ± 1.26	32.44 ± 2.27	91.12 ± 1.42
A13	9.54 ± 0.72	24.82 ± 0.91	>100	7.25 ± 0.49	218.94 ± 0.47
A14	17.85 ± 0.58	21.98 ± 1.24	21.06 ± 0.89	29.24 ± 0.27	165.21 ± 2.18
A15	27.62 ± 0.21	>100	7.42 ± 0.58	30.61 ± 1.08	95.77 ± 2.63
A16	45.32 ± 1.63	18.35 ± 0.72	22.97 ± 0.13	>100	152.38 ± 0.45
A17	25.05 ± 0.25	>100	32.36 ± 0.95	27.39 ± 1.05	171.59 ± 1.27
A18	41.24 ± 1.61	>100	23.91 ± 0.52	28.67 ± 0.67	153.72 ± 1.94
A19	>100	27.04 ± 1.86	26.14 ± 0.27	>100	211.02 ± 2.05
A20	22.56 ± 0.78	>100	40.35 ± 2.01	>100	>300
A21	14.05 ± 1.25	20.61 ± 0.43	21.58 ± 0.81	18.45 ± 0.12	197.83 ± 1.18
A22	24.88 ± 2.16	>100	8.74 ± 0.65	19.33 ± 0.55	143.37 ± 1.51
A23	9.71 ± 0.47	16.43 ± 0.62	2.34 ± 0.27	12.51 ± 1.18	205.95 ± 2.36
A24	12.39 ± 1.08	8.52 ± 0.94	13.16 ± 0.78	10.75 ± 0.53	171.54 ± 1.29
A25	>100	31.65 ± 0.39	23.13 ± 1.35	18.84 ± 1.05	139.26 ± 2.24
Celecoxib	28.85 ± 1.27	83.49 ± 0.61	25.72 ± 0.26	29.25 ± 1.91	182.32 ± 1.08
Cisplatin	10.06 ± 0.54	23.18 ± 0.83	8.73 ± 1.09	28.36 ± 0.43	89.27 ± 2.15

[a] IC_{50}: The concentration of compounds inhibits 50% of cell growth. Data are shown as the mean ± SD of three independent experiments (n = 3).

[M+H] $^{+}$. Anal. Calcd for $C_{27}H_{28}FN_4O_6PS$: C, 55.29; H, 4.81; N, 9.55.

*4.5.2. Diethyl((4-bromophenyl)(5-(4-fluorophenyl)-1-(4-sulfamoylphenyl)-1H-pyrazole-3-carboxamido)methyl)phosphonate (**A2**)*

White solid, yield 59.6%, m.p.: 92.5–93.7 °C. ^{1}H NMR (600 MHz, DMSO-d_6) δ 8.81 (dd, J = 9.6, 3.5 Hz, 1H), 7.91 (d, J = 8.6 Hz, 2H), 7.62–7.55 (m, 6H), 7.54 (s, 2H), 7.38 (dd, J = 8.5, 5.3 Hz, 2H), 7.28 (t, J = 8.8 Hz, 2H), 7.17 (s, 1H), 5.71 (dd, J = 22.0, 9.7 Hz, 1H), 4.11–4.04 (m, 2H), 3.98 (s, 1H), 3.91 (dd, J = 16.7, 9.2 Hz, 1H), 1.21 (t, J = 7.1 Hz, 3H), 1.13 (t, J = 7.0 Hz, 3H). ESI-MS: 665.06 [M+H] $^{+}$. Anal. Calcd for $C_{27}H_{27}BrFN_4O_6PS$: C, 48.73; H, 4.09; N, 8.42.

*4.5.3. Diethyl((5-(3-fluorophenyl)-1-(4-sulfamoylphenyl)-1H-pyrazole-3-carboxamido)(phenyl)methyl)phosphonate (**A3**)*

Light yellow solid, yield 64.1%, m.p.: 105.1–105.6 °C. ^{1}H NMR (600 MHz, DMSO-d_6) δ 8.72 (dd, J = 9.8, 3.5 Hz, 1H), 7.90 (d, J = 8.6 Hz, 2H), 7.59 (dd, J = 16.3, 8.2 Hz, 4H), 7.53 (s, 2H), 7.45 (d, J = 6.2 Hz, 1H), 7.38 (t, J = 7.6 Hz, 2H), 7.33 (s, 1H), 7.23 (s, 3H), 7.09 (d, J = 7.8 Hz, 1H), 5.68 (dd, J = 21.7, 9.8 Hz, 1H), 4.06 (d, J = 7.2 Hz, 2H), 3.94 (s, 1H), 3.86–3.80 (m, 1H), 1.20 (t, J = 7.0 Hz, 3H), 1.09 (t, J = 7.0 Hz, 3H). ESI-MS: 587.15 [M+H]+. Anal. Calcd for: $C_{27}H_{28}FN_4O_6PS$ C, 55.29; H, 4.81; N, 9.55.

*4.5.4. Diethyl((4-bromophenyl)(5-(3-fluorophenyl)-1-(4-sulfamoylphenyl)-1H-pyrazole-3-carboxamido)methyl)phosphonate(**A4**)*

Yellow solid, yield 53.8%, m.p.: 90.1–90.7 °C. ^{1}H NMR (600 MHz, DMSO-d_6) δ 8.81 (dd, J = 9.7, 3.7 Hz, 1H), 7.89 (d, J = 11.0 Hz, 2H), 7.60–7.57 (m, 3H), 7.54 (d, J = 7.0 Hz, 2H), 7.52 (s, 2H), 7.44 (d, J = 22.1 Hz, 2H), 7.29–7.20 (m, 3H), 7.09 (d, J = 7.8 Hz, 1H), 5.68 (dd, J = 22.0, 9.7 Hz, 1H), 4.10–4.04 (m, 2H), 3.99–3.95 (m, 1H), 3.91–3.86 (m, 1H), 1.20 (t, J = 7.0 Hz, 3H), 1.12 (t, J = 7.0 Hz, 3H). ESI-MS: 665.06 [M+H] $^{+}$. Anal. Calcd for $C_{27}H_{27}BrFN_4O_6PS$: C, 48.73; H, 4.09; N, 8.42.

*4.5.5. Diethyl((5-(2-fluorophenyl)-1-(4-sulfamoylphenyl)-1H-pyrazole-3-carboxamido) (phenyl)methyl)phosphonate(**A5**)*

Yellow solid, yield 75.4%, m.p.: 87.5–88.4 °C. ^{1}H NMR (600 MHz, DMSO-d_6) δ 8.80 (dd, J = 9.8, 3.4 Hz, 1H), 7.83 (d, J = 8.7 Hz, 2H), 7.60 (d, J = 7.7 Hz, 2H), 7.51 (d, J = 8.7 Hz, 5H), 7.48 (d, J = 6.9 Hz, 3H), 7.39 (t, J = 7.4 Hz, 2H), 7.33 (t, J = 7.8 Hz, 1H), 7.13 (s, 1H), 5.70 (dd, J = 21.7, 9.8 Hz, 1H), 4.10–4.03 (m, 2H), 3.98–3.93 (m, 1H), 3.87–3.81 (m, 1H), 1.21 (t, J = 7.0 Hz, 3H), 1.09 (t, J = 7.0 Hz, 3H). ESI-MS: 587.15 [M+H] $^{+}$. Anal. Calcd for $C_{27}H_{28}FN_4O_6PS$: C, 55.29; H, 4.81; N, 9.55.

*4.5.6. Diethyl((4-bromophenyl)(5-(2-fluorophenyl)-1-(4-sulfamoylphenyl)-1H-pyrazol-3-carboxamido)methyl)phosphonate(**A6**)*

Yellow solid, yield 52.7%, m.p.: 93.2–94.6 °C. ^{1}H NMR (600 MHz, DMSO-d_6) δ 8.88 (dd, J = 9.7, 3.5 Hz, 1H), 7.86 (d, J = 8.6 Hz, 2H), 7.61–7.53 (m, 7H), 7.50 (s, 3H), 7.32 (t, J = 7.9 Hz, 1H), 7.29–7.25 (m, 1H), 7.18 (s, 1H), 5.70 (dd, J = 22.0, 9.7 Hz, 1H), 4.10–4.03 (m, 2H), 4.00–3.95 (m, 1H), 3.90 (dd, J = 16.6, 9.4 Hz, 1H), 1.21 (t, J = 7.0 Hz, 3H), 1.12 (t, J = 7.0 Hz, 3H). ESI-MS: 665.06 [M+H] $^{+}$. Anal. Calcd for $C_{27}H_{27}BrFN_4O_6PS$: C, 48.73; H, 4.09; N, 8.42.

*4.5.7. Diethyl((5-(4-chlorophenyl)-1-(4-sulfamoylphenyl)-1H-pyrazole-3-carboxamido)(phenyl)methyl)phosphonate(**A7**)*

Yellow solid, yield 56.0%, m.p.: 86.1–86.9 °C. ^{1}H NMR (600 MHz, DMSO-d_6) δ 8.72 (dd, J = 9.7, 3.2 Hz, 1H), 7.90 (d, J = 8.6 Hz, 2H), 7.68–7.59 (m, 4H), 7.58 (d, J = 7.8 Hz, 2H), 7.53 (s, 2H), 7.38 (t, J = 7.7 Hz, 2H), 7.33 (q, J = 7.4, 6.8 Hz, 2H), 7.25 (s, 1H), 7.21 (d, J = 7.9 Hz, 1H), 5.68 (dd, J = 21.7, 9.8 Hz, 1H), 4.09–4.02 (m, 2H), 3.97–3.92 (m, 1H), 3.83 (dd, J = 17.3, 8.6 Hz, 1H), 1.20 (t, J = 7.0 Hz, 3H), 1.09 (t, J = 7.0 Hz, 3H). ESI-MS: 603.12 [M+H] $^{+}$. Anal. Calcd for $C_{27}H_{28}ClN_4O_6PS$: C, 53.78; H, 4.68; N, 9.29.

*4.5.8. Diethyl((4-bromophenyl)(5-(4-chlorophenyl)-1-(4-sulfamoylphenyl)-1H-pyrazole-3-carboxamido)methyl)phosphonate(**A8**)*

White solid, yield 60.8%, m.p.: 102.3–104.2 °C. ^{1}H NMR (600 MHz, DMSO-d_6) δ 8.83 (dd, J = 9.7, 3.7 Hz, 1H), 7.91 (d, J = 8.6 Hz, 2H), 7.60 (d, J = 11.9 Hz, 4H), 7.56 (d, J = 7.5 Hz, 2H), 7.53 (s, 2H), 7.50 (d, J = 8.5 Hz, 2H), 7.34 (d, J = 8.5 Hz, 2H), 7.20 (s, 1H), 5.70 (dd, J = 22.0, 9.7 Hz, 1H), 4.11–4.04 (m, 2H), 4.01–3.95 (m, 1H), 3.93–3.87 (m, 1H), 1.21 (t, J = 7.0 Hz, 3H), 1.13 (t, J = 7.0 Hz, 3H). ESI-MS: 681.03 [M+H] $^{+}$. Anal. Calcd for $C_{27}H_{27}BrClN_4O_6PS$: C, 47.56; H, 3.99; N, 8.22.

*4.5.9. Diethyl((5-(3-chlorophenyl)-1-(4-sulfamoylphenyl)-1H-pyrazole-3-carboxamido)(phenyl)methyl)phosphonate(**A9**)*

White solid, yield 80.2%, m.p.: 125.4–126.5 °C. ^{1}H NMR (600 MHz,

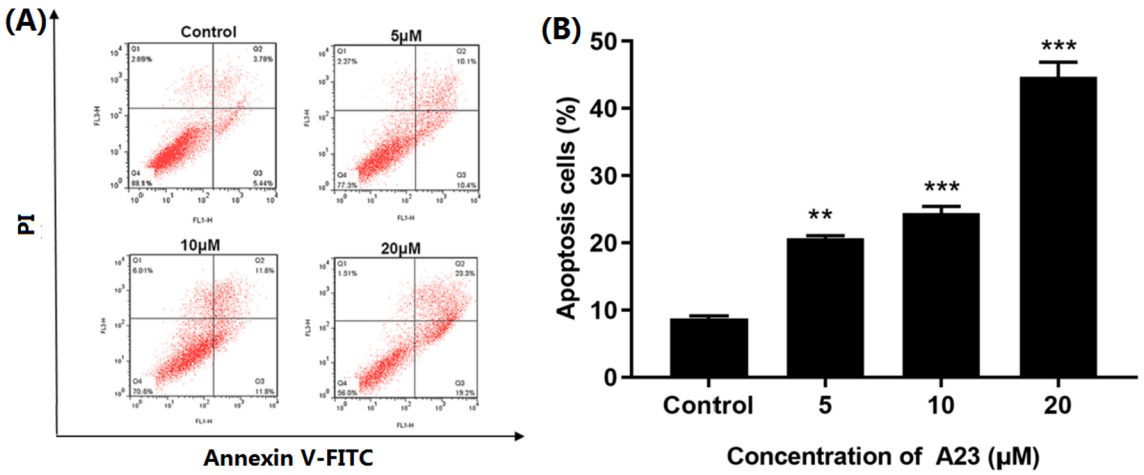

Fig. 4. Hit compound **A23** induced apoptosis in HCT116 cells. (A) The result of HCT116 cells treated with different concentrations of **A23** (0, 5, 10, and 20 μM) for 48 h; (B) Apoptotic ratios of HCT116 cells. Data are shown as mean ± SD of three independent experiments; $^{**}p < 0.01$, $^{***}p < 0.001$. Statistical analyses performed with a two-tailed Student's *t*-test with unequal variance.

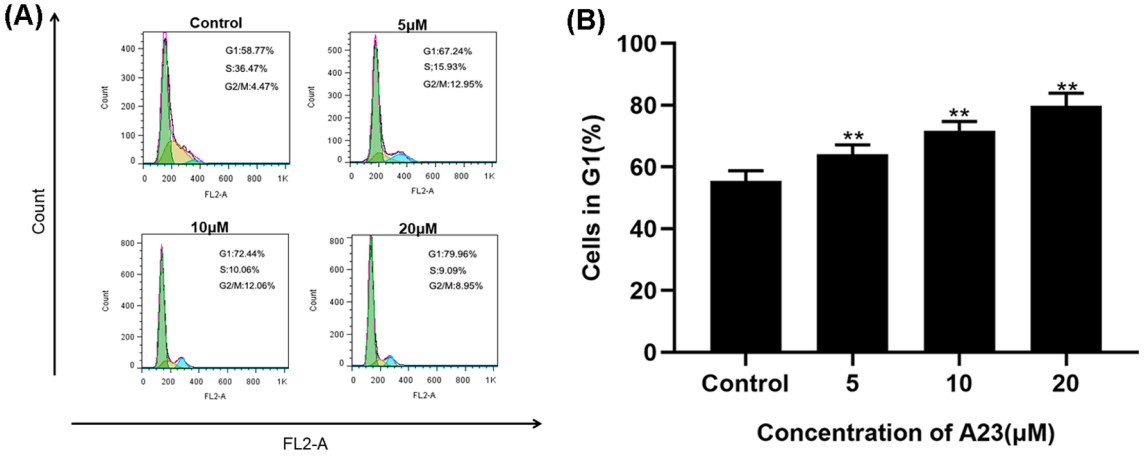

Fig. 5. (A) The variations in cell cycle of HCT116 cells with treatment of hit compound **A23**. (B) The percentage of cells in the G1 phase. Data are shown as mean ± SD of three independent experiments; $^{*}p < 0.05$, $^{**}p < 0.01$. Statistical analyses performed with a two-tailed Student's t-test with unequal variance.

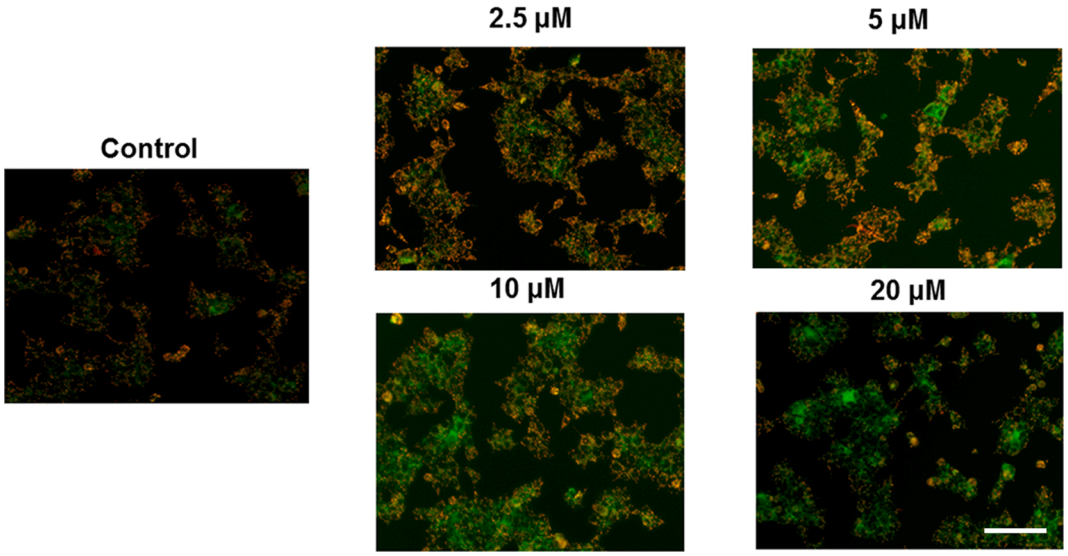

Fig. 6. Effect of compound **A23** on mitochondrial membrane potential of HCT116 cells. Scale bar: 100 μm.

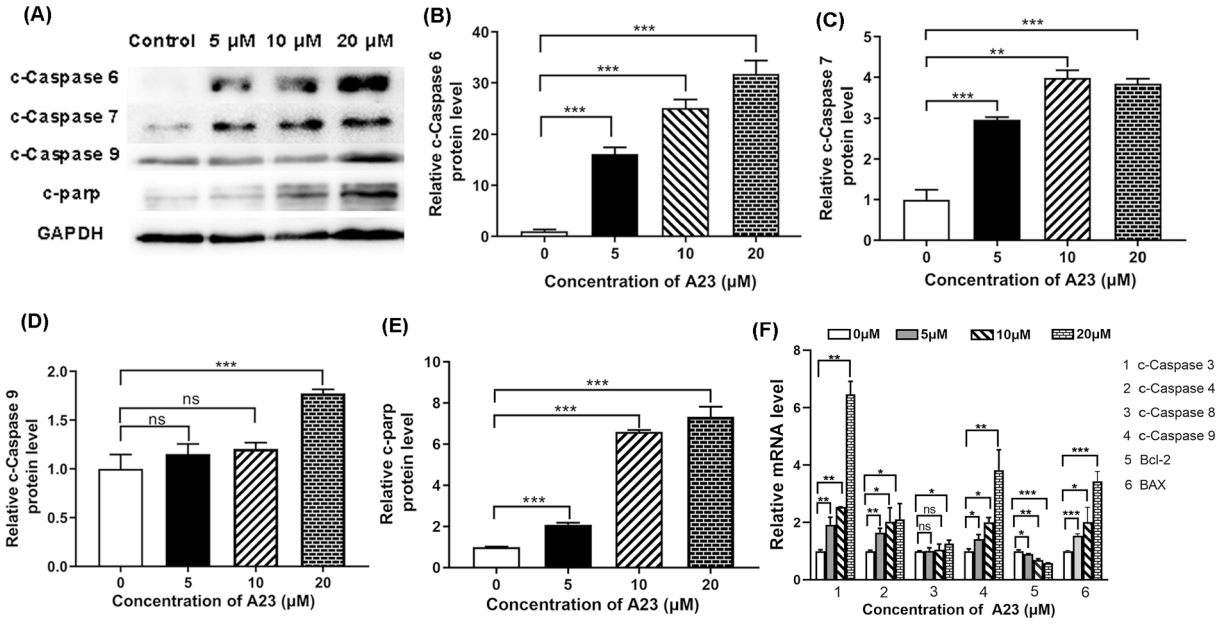

Fig. 7. Effects of compound A23 after treatment for 48h on HCT116 cells detected by qRT-PCR and Western blotting. Statistical analyses performed with a two-tailed Student's t-test with unequal variance.

DMSO-d_6) δ 8.71 (dd, J = 9.8, 3.6 Hz, 1H), 7.90 (d, J = 8.6 Hz, 2H), 7.62–7.54 (m, 4H), 7.54–7.46 (m, 4H), 7.38 (t, J = 7.7 Hz, 2H), 7.33 (d, J = 8.5 Hz, 3H), 7.20 (s, 1H), 5.68 (dd, J = 21.7, 9.8 Hz, 1H), 4.10–4.01 (m, 2H), 3.97–3.91 (m, 1H), 3.87–3.80 (m, 1H), 1.20 (t, J = 7.0 Hz, 3H), 1.09 (t, J = 7.0 Hz, 3H). ESI-MS: 603.12 [M+H] $^+$. Anal. Calcd for $C_{27}H_{28}ClN_4O_6PS$: C, 53.78; H, 4.68; N, 9.29.

*4.5.10. Diethyl((4-bromophenyl)(5-(3-chlorophenyl)-1-(4-sulfamoylphenyl)-1H-pyrazole-3-carboxamido)methyl)phosphonate(**A10**)*

White solid, yield 51.9%, m.p.: 112.7–113.9 °C. ^{1}H NMR (600 MHz, DMSO-d_6) δ 8.95–8.73 (m, 1H), 7.92 (d, J = 8.4 Hz, 2H), 7.69–7.61 (m, 4H), 7.60–7.49 (m, 6H), 7.35 (t, J = 7.8 Hz, 1H), 7.30–7.12 (m, 2H), 5.71 (dd, J = 21.9, 9.6 Hz, 1H), 4.14–4.04 (m, 2H), 4.03–3.95 (m, 1H), 3.90 (q, J = 9.3, 8.8 Hz, 1H), 1.21 (t, J = 7.0 Hz, 3H), 1.13 (t, J = 7.0 Hz, 3H). ESI-MS: 681.03 [M+H] $^+$. Anal. Calcd for $C_{27}H_{27}BrClN_4O_6PS$: C, 47.56; H, 3.99; N, 8.22.

*4.5.11. Diethyl((5-(2-chlorophenyl)-1-(4-sulfamoylphenyl)-1H-pyrazole-3-carboxamio)(phenyl)methyl)phosphonate(**A11**)*

Yellow solid, yield 78.4%, m.p.: 88.5–90.3 °C. ^{1}H NMR (600 MHz, DMSO-d_6) δ 8.82 (dd, J = 9.8, 3.3 Hz, 1H), 7.83 (d, J = 8.6 Hz, 2H), 7.59 (dd, J = 13.7, 7.0 Hz, 3H), 7.54–7.46 (m, 7H), 7.39 (t, J = 7.5 Hz, 2H), 7.33 (t, J = 7.2 Hz, 1H), 7.13 (s, 1H), 5.70 (dd, J = 21.7, 9.8 Hz, 1H), 4.10–4.04 (m, 2H), 3.98–3.93 (m, 1H), 3.87–3.82 (m, 1H), 1.21 (t, J = 7.0 Hz, 3H), 1.09 (t, J = 7.0 Hz, 3H). ESI-MS: 603.12 [M+H]+. Anal. Calcd for $C_{27}H_{28}ClN_4O_6PS$: C, 53.78; H, 4.68; N, 9.29.

*4.5.12. Diethyl((4-bromophenyl)(5-(2-chlorophenyl)-1-(4-sulfamoylphenyl)-1H-pyrazole-3-carboxamido)methyl)phosphonate(**A12**)*

Yellow solid, yield 67.1%, m.p.: 91.8–93.4 °C. ^{1}H NMR (600 MHz, DMSO-d_6) δ 8.89 (dd, J = 9.7, 3.6 Hz, 1H), 7.98 (d, J = 8.4 Hz, 1H), 7.83 (d, J = 8.7 Hz, 2H), 7.72 (d, J = 8.3 Hz, 1H), 7.61–7.54 (m, 4H), 7.54 (d, J = 1.5 Hz, 1H), 7.52–7.38 (m, 5H), 7.12 (s, 1H), 5.70 (dd, J = 21.9, 9.7 Hz, 1H), 4.08 (dd, J = 12.4, 7.9 Hz, 2H), 3.98 (dd, J = 8.8, 5.9 Hz, 1H), 3.90 (dd, J = 18.1, 8.0 Hz, 1H), 1.21 (t, J = 7.0 Hz, 3H), 1.12 (t, J = 7.0 Hz, 3H). ESI-MS: 681.03 [M+H] $^+$. Anal. Calcd for $C_{27}H_{27}BrClN_4O_6PS$: C, 47.56; H,3.99; N, 8.22.

*4.5.13. Diethyl(1-(5-(4-bromophenyl)-1-(4-sulfamoylphenyl)-1H-pyrazole-3-carboxamido)ethyl)phosphonate(**A13**)*

Yellow solid, yield 6.2%, m.p.: 143.2–143.7 °C. ^{1}H NMR (600 MHz, DMSO-d_6) δ 8.38 (d, J = 9.3 Hz, 1H), 7.93 (d, J = 8.4 Hz, 2H), 7.67 (d, J = 8.3 Hz, 2H), 7.61 (d, J = 8.5 Hz, 2H), 7.55 (s, 2H), 7.31 (d, J = 8.3 Hz, 2H), 7.19 (s, 1H), 4.58 (dd, J = 15.6, 7.9 Hz, 1H), 4.10 (dd, J = 16.0, 9.1 Hz, 4H), 1.43 (dd, J = 11.9, 4.7 Hz, 3H), 1.29–1.26 (m, 6H). ESI-MS: 585.05 [M+H] $^+$. Anal. Calcd for $C_{22}H_{26}BrN_4O_6PS$: C, 45.14; H, 4.48; N, 9.57.

*4.5.14. Diethyl((5-(4-bromophenyl)-1-(4-sulfamoylphenyl)-1H-pyrazole-3-carboxamido)(phenyl)methyl)phosphonate(**A14**)*

Light yellow solid, yield 58.3%, m.p.: 102.4–103.6 °C. ^{1}H NMR (600 MHz, DMSO-d_6) δ 8.74–8.68 (m, 1H), 7.89 (d, J = 8.4 Hz, 2H), 7.69–7.54 (m, 6H), 7.51 (s, 2H), 7.35 (dt, J = 33.6, 7.3 Hz, 3H), 7.26 (d, J = 8.3 Hz, 2H), 7.20 (s, 1H), 5.70–5.64 (m, 1H), 4.09–4.02 (m, 2H), 3.96–3.91 (m, 1H), 3.86–3.80 (m, 1H), 1.20 (t, J = 7.0 Hz, 3H), 1.09 (t, J = 7.0 Hz, 3H). ESI-MS: 647.07 [M+H] $^+$. Anal. Calcd for $C_{27}H_{28}BrN_4O_6PS$: C, 50.09; H, 4.36; N, 8.65.

*4.5.15. Diethyl((4-bromophenyl)(5-(4-bromophenyl)-1-(4-sulfamoylphenyl)-1H-pyrazole-3-carboxamido)methyl)phosphonate(**A15**)*

Yellow solid, yield 63.5%, m.p.: 95.3–96.9 °C. ^{1}H NMR (600 MHz, DMSO-d_6) δ 8.81 (dd, J = 9.7, 3.7 Hz, 1H), 7.89 (d, J = 8.6 Hz, 2H), 7.63 (d, J = 8.5 Hz, 2H), 7.61–7.56 (m, 4H), 7.56–7.53 (m, 2H), 7.51 (s, 2H), 7.26 (d, J = 8.5 Hz, 2H), 7.20 (s, 1H), 5.68 (dd, J = 22.0, 9.7 Hz, 1H), 4.10–4.03 (m, 2H), 3.96 (d, J = 7.4 Hz, 1H), 3.89 (dd, J = 16.6, 9.5 Hz, 1H), 1.20 (t, J = 7.0 Hz, 3H), 1.12 (t, J = 7.0 Hz, 3H). ESI-MS: 724.98 [M+H] $^+$. Anal. Calcd for $C_{27}H_{27}Br_2N_4O_6PS$: C, 44.65; H, 3.75; N, 7.71.

*4.5.16. Diethyl(phenyl(1-(4-sulfamoylphenyl)-5-(4-(trifluoromethyl)phenyl)-1H-pyrazole-3-carboxamido)methyl)phosphonate(**A16**)*

Yellow solid, yield 65.7%, m.p.: 76.9–77.4 °C. ^{1}H NMR (600 MHz, DMSO-d_6) δ 8.76 (dd, J = 9.8, 3.5 Hz, 1H), 7.91 (d, J = 8.6 Hz, 2H), 7.80 (d, J = 8.2 Hz, 2H), 7.61 (d, J = 8.6 Hz, 2H), 7.59–7.56 (m, 2H), 7.54 (d, J = 8.3 Hz, 4H), 7.39 (t, J = 7.7 Hz, 3H), 7.30 (s, 1H), 5.68 (dd, J = 21.7, 9.8 Hz, 1H), 4.06 (q, J = 8.8, 8.4 Hz, 2H), 3.97–3.92 (m, 1H), 3.84 (dd, J = 16.5, 9.4 Hz, 1H), 1.20 (t, J = 7.0 Hz, 3H), 1.09 (t, J = 7.0 Hz, 3H). ESI-MS: 637.14 [M+H] $^+$. Anal. Calcd for $C_{28}H_{28}F_3N_4O_6PS$: C, 52.83; H, 4.43; N, 8.80.

*4.5.17. Diethyl ((4-bromophenyl)(1-(4-sulfamoylphenyl)-5-(4-(trifluoromethyl)phenyl)-1H-pyrazole-3-carboxamido)methyl)phosphonate (**A17**)*

Yellow solid, yield 82.6%, m.p.: 109.5–110.2 °C. ^{1}H NMR (600 MHz, DMSO-d_6) δ 8.87 (dd, J = 9.7, 3.6 Hz, 1H), 7.95–7.90 (m, 2H), 7.80 (d, J = 8.3 Hz, 2H), 7.68–7.58 (m, 4H), 7.55 (d, J = 11.3 Hz, 6H), 7.30 (s, 1H), 5.71 (dd, J = 22.0, 9.7 Hz, 1H), 4.12–4.04 (m, 2H), 4.03–4.00 (m, 1H), 3.91 (dd, J = 9.5, 6.3 Hz, 1H), 1.21 (t, J = 7.1 Hz, 3H), 1.13 (t, J = 7.2 Hz, 3H). ESI-MS: 715.05 [M+H] $^+$. Anal. Calcd for $C_{28}H_{27}BrF_3N_4O_6PS$: C, 47.00; H, 3.80; N, 7.83.

*4.5.18. Diethyl(1-(1-(4-sulfamoylphenyl)-5-(p-tolyl)-1H-pyrazole-3-carboxamido)ethyl)phosphonate(**A18**)*

Yellow solid, yield 8.4%, m.p.: 135.8–136.3 °C. ^{1}H NMR (600 MHz, DMSO-d_6) δ 8.19 (d, J = 9.7 Hz, 1H), 7.87 (d, J = 8.6 Hz, 2H), 7.55 (d, J = 8.6 Hz, 2H), 7.50 (s, 2H), 7.21 (q, J = 8.2 Hz, 4H), 7.07 (s, 1H), 4.33 (dd, J = 10.0, 4.8 Hz, 1H), 4.04 (dd, J = 16.1, 8.9 Hz, 4H), 2.32 (s, 3H), 1.84–1.75 (m, 2H), 1.22 (dt, J = 19.1, 7.0 Hz, 6H), 0.91 (t, J = 7.3 Hz, 3H). ESI-MS: 521.15 [M+H] $^+$. Anal. Calcd for $C_{23}H_{29}N_4O_6PS$: C, 53.07; H, 5.62; N, 10.76.

*4.5.19. Diethyl(phenyl(1-(4-sulfamoylphenyl)-5-(p-tolyl)-1H-pyrazole-3-carboxamido)methyl)phosphonate(**A19**)*

White solid, yield 70.3%, m.p.: 121.4–122.6 °C. ^{1}H NMR (600 MHz, DMSO-d_6) δ 8.67 (dd, J = 9.8, 3.6 Hz, 1H), 7.88 (d, J = 8.6 Hz, 2H), 7.57 (d, J = 8.6 Hz, 4H), 7.51 (s, 2H), 7.38 (t, J = 7.6 Hz, 2H), 7.33 (d, J = 6.5 Hz, 1H), 7.25–7.15 (m, 4H), 7.11 (s, 1H), 5.67 (dd, J = 21.7, 9.8 Hz, 1H), 4.09–4.02 (m, 2H), 3.97–3.92 (m, 1H), 3.83 (dd, J = 17.3, 8.6 Hz, 1H), 2.31 (s, 3H), 1.21 (s, 3H), 1.08 (s, 3H). ESI-MS: 583.17 [M+H] $^+$. Anal. Calcd for $C_{28}H_{31}N_4O_6PS$: C, 57.72; H, 5.36; N, 9.62.

*4.5.20. Diethyl((4-bromophenyl)(1-(4-sulfamoylphenyl)-5-(p-tolyl)-1H-pyrazole-3-carboxamido)methyl)phosphonate(**A20**)*

White solid, yield 77.4%, m.p.: 118.3–120.7 °C. ^{1}H NMR (600 MHz, DMSO-d_6) δ 8.79 (dd, J = 9.5, 3.2 Hz, 1H), 7.90 (d, J = 8.5 Hz, 2H), 7.62–7.51 (m, 8H), 7.21 (q, J = 8.0 Hz, 4H), 7.12 (s, 1H), 5.70 (dd, J = 21.9, 9.7 Hz, 1H), 4.12–4.04 (m, 2H), 4.02–3.95 (m, 1H), 3.90 (q, J = 9.7, 9.0 Hz, 1H), 2.32 (s, 3H), 1.21 (t, J = 7.0 Hz, 3H), 1.13 (t, J = 7.0 Hz, 3H). ESI-MS: 661.08 [M+H] $^+$. Anal. Calcd for $C_{28}H_{30}BrN_4O_6PS$: C, 50.84; H, 4.57; N, 8.47.

*4.5.21. Diethyl((5-(4-methoxyphenyl)-1-(4-sulfamoylphenyl)-1H-pyrazole-3-carboxamido)(phenyl)methyl)phosphonate(**A21**)*

Yellow solid, yield 55.2%, m.p.: 98.5–99.6 °C. ^{1}H NMR (600 MHz, DMSO-d_6) δ 8.65 (dd, J = 9.8, 3.6 Hz, 1H), 7.89 (d, J = 8.6 Hz, 2H), 7.62–7.55 (m, 4H), 7.52 (s, 2H), 7.38 (t, J = 7.5 Hz, 2H), 7.33 (t, J = 7.7 Hz, 1H), 7.23 (d, J = 8.8 Hz, 2H), 7.08 (s, 1H), 6.97 (d, J = 8.8 Hz, 2H), 5.67 (dd, J = 21.7, 9.8 Hz, 1H), 4.09–4.03 (m, 2H), 3.97–3.92 (m, 1H), 3.83 (dd, J = 10.2, 1.5 Hz, 1H), 3.77 (s, 3H), 1.20 (t, J = 7.0 Hz, 3H), 1.09 (t, J = 7.0 Hz, 3H). ESI-MS: 599.17[M+H] $^+$. Anal. Calcd for $C_{28}H_{31}N_4O_7PS$: C, 56.18; H, 5.22; N, 9.36.

*4.5.22. Diethyl((4-bromophenyl)(5-(4-methoxyphenyl)-1-(4-sulfamoylphenyl)-1H-pyrazole-3-carboxamido)methyl)phosphonate(**A22**)*

Yellow solid, yield 79.8%, m.p.: 85.9–87.2 °C. ^{1}H NMR (600 MHz, DMSO-d_6) δ 8.75 (dd, J = 9.7, 3.7 Hz, 1H), 7.89 (d, J = 8.7 Hz, 2H), 7.65–7.56 (m, 4H), 7.56–7.51 (m, 4H), 7.23 (d, J = 8.8 Hz, 2H), 7.07 (s, 1H), 6.97 (d, J = 8.8 Hz, 2H), 5.69 (dd, J = 22.0, 9.7 Hz, 1H), 4.10–4.03 (m, 2H), 4.01–3.97 (m, 1H), 3.90 (dd, J = 9.5, 7.7 Hz, 1H), 3.77 (s, 3H), 1.20 (t, J = 7.0 Hz, 3H), 1.12 (t, J = 7.0 Hz, 3H). ESI-MS: 677.08 [M+H] $^+$. Anal. Calcd for $C_{28}H_{30}BrN_4O_7PS$: C, 49.64; H, 4.46; N, 8.27.

*4.5.23. Diethyl(1-(5-(3-methoxyphenyl)-1-(4-sulfamoylphenyl)-1H-pyrazole-3-carboxamido)ethyl)phosphonate(**A23**)*

Yellow solid, yield 5.1%, m.p.: 108.6–110.3 °C. ^{1}H NMR (400 MHz, DMSO-d_6) δ 8.30 (d, J = 9.4 Hz, 1H), 7.88 (d, J = 8.7 Hz, 2H), 7.60–7.49 (m, 4H), 7.31 (t, J = 8.0 Hz, 1H), 7.13 (s, 1H), 6.98 (dd, J = 8.3, 2.0 Hz, 1H), 6.89 (d, J = 2.3 Hz, 1H), 6.81 (d, J = 7.9 Hz, 1H), 4.66–4.40 (m, 1H), 4.11–4.01 (m, 4H), 3.69 (s, 3H), 1.37 (dd, J = 16.6, 7.4 Hz, 3H), 1.24 (dt, J = 11.8, 7.0 Hz, 6H). ESI-MS: 537.15 [M+H] $^+$. Anal. Calcd for $C_{23}H_{29}N_4O_7PS$: C, 51.49; H, 5.45; N, 10.44.

*4.5.24. Diethyl((5-(3-methoxyphenyl)-1-(4-sulfamoylphenyl)-1H-pyrazole-3-carboxamido)(phenyl)methyl)phosphonate(**A24**)*

Yellow solid, yield 59.0%, m.p.: 130.1–130.8 °C. ^{1}H NMR (600 MHz, DMSO-d_6) δ 8.69 (dd, J = 9.8, 3.5 Hz, 1H), 7.90 (d, J = 8.6 Hz, 2H), 7.64–7.55 (m, 4H), 7.53 (s, 2H), 7.39 (t, J = 7.6 Hz, 2H), 7.32 (dt, J = 15.9, 7.6 Hz, 2H), 7.19 (s, 1H), 6.98 (dd, J = 8.3, 2.0 Hz, 1H), 6.89 (s, 1H), 6.81 (d, J = 7.7 Hz, 1H), 5.68 (dd, J = 21.7, 9.8 Hz, 1H), 4.06 (q, J = 8.7, 8.3 Hz, 2H), 3.98–3.91 (m, 1H), 3.84 (q, J = 8.7 Hz, 1H), 3.69 (s, 3H), 1.20 (t, J = 7.0 Hz, 3H), 1.09 (t, J = 7.0 Hz, 3H). ESI-MS: 599.17 [M+H] $^+$. Anal. Calcd for $C_{28}H_{31}N_4O_7PS$: C, 56.18; H, 5.22; N, 9.36.

*4.5.25. Diethyl((4-bromophenyl)(5-(3-methoxyphenyl)-1-(4-sulfamoylphenyl)-1H-pyrazole-3-carboxamido)methyl)phosphonate(**A25**)*

Yellow solid, yield 62.5%, m.p.: 78.3–79.2 °C. ^{1}H NMR (600 MHz, DMSO-d_6) δ 8.79 (dd, J = 9.5, 3.2 Hz, 1H), 7.90 (d, J = 8.5 Hz, 2H), 7.62–7.51 (m, 8H), 7.21 (q, J = 8.0 Hz, 4H), 7.12 (s, 1H), 5.70 (dd, J = 21.9, 9.7 Hz, 1H), 4.12–4.04 (m, 2H), 4.02–3.95 (m, 1H), 3.90 (q, J = 9.7, 9.0 Hz, 1H), 2.32 (s, 3H), 1.21 (t, J = 7.0 Hz, 3H), 1.13 (t, J = 7.0 Hz, 3H). ESI-MS: 677.08 [M+H] $^+$. Anal. Calcd for $C_{28}H_{30}BrN_4O_7PS$: C, 49.64; H, 4.46; N, 8.27.

4.6. Cell culture

HeLa (Human epithelial cervical cancer cell line), MCF-7 (human breast cancer cell line), HCT116 (human colon cancer cell line), HepG2 (human hepatoma cell line), and 293T (human embryonic kidney cell line) were cultivated in Dulbecco's modified Eagle's medium (DMEM), supplemented with 10% fetal bovine serum (FBS, BI), 100 U/mL penicillin and 100 mg/mL streptomycin, and maintained in a humidified incubator with 5% CO_2 at 37 °C。

4.7. COX inhibition assay

The inhibitory ability of the synthesized compounds on COX-1 and COX-2 was determined by COX-1/COX-2 ELISA Kit. COX-1 or COX-2 enzyme was pre-incubated with test compounds at various concentrations in the supplied buffer (0.1 M Tris–HCl, pH 8.0, 5 mM EDTA, 2 mM phenol and 1 μM heme) for 10 min at 37 °C. 10 μL arachidonic acid (100 μM) was added to initiate the reactions, which incubated 2 min at 37 °C. Then the reaction was stopped by adding 50 μL of 1 M HCl, following by one-tenth the volume of saturated stannous chloride (50 mg/mL). The reaction mixture was incubated at room temperature for 5 min. According to the detection method of the kit, the wavelength of each well at 450 nm was measured by enzyme immunoassay [30].

4.8. Anti-proliferation assay

The anti-proliferative activity of the synthesized products against HeLa, MCF-7, HCT116, HepG2 and 293T cell lines was assessed using a modified standard (MTT) – based colorimetric assay. The cells grown to log phase were plated at a density of 5000 cells per well on a 96-well plate and treated with gradient concentrations (0.01, 0.1, 1, 10 and 100 μM) of tested compounds for 48 h. After that, MTT (10 mg/ mL) (Sigma, USA) added and incubated for 4 h at 37 °C. 150 μL DMSO was added in each well and shaken for 5 min. The absorbance (OD 570 nm) was measured at a wavelength of 630 nm on an ELISA reader (ELx800, BioTek, USA). IC_{50} values of compounds were calculated by comparison with DMSO treated control wells. Each drug concentration was repeated in three wells. Each assay was carried out three times for each cell line.

4.9. Cell apoptosis assay

HCT116 cells were plated six-well plates at 10^6/well, and treated with compound A23 at final concentrations of 0, 5, 10, and 20 μM for 48 h. The cells were collected by trypsin, washed with PBS and resuspend into 500 μL of binding buffer. Then Annexin-V/FITC (5 μL) and PI (5 μL) were added to the above buffer and incubated for 15 min at RT (25 °C) away from light. The cell apoptosis was analyzed with FACS Calibur flow cytometer (Becton Dickinson, San Jose, CA, USA). Statistical analysis was performed with the Flowjo 7.6.1 software (Emerald Biotech Co. Ltd., Hangzhou, China).

4.10. Cell cycle assay

HCT116 cells were treated with compound **A23** at indicated concentrations (0, 5, 10, and 20 μM) for 48 h, washed twice with ice-cold PBS and fixed with 70% ethanol at 4 °C overnight. The cells were centrifuged at 4000 rpm and treated with RNase A (0.1 mg/mL). After incubation at 37 °C for 30 min, 400 μL propidium iodide (PI) was mixed with the cells. Analysis was performed with FACSCalibur flow cytometer (Becton Dickinson, San Jose, CA, USA).

4.11. Mitochondrial membrane potential evaluation

Mitochondrial depolarization in HCT116 cells were measured by JC-1 dye (CBIC2(3), Beyotime, Haimen, China). HCT116 cells grown in six-well plates were treated with different concentrations (0, 2.5, 5, 10, and 20 μM) of compound **A23** for 24 h. Then the culture medium was removed and HCT116 cells were stained with JC-1 staining solution (5 mg/mL) for 20 min. After being washed twice with PBS, the stained cells were observed fluorescence microscope (OLYMPUS IX71) [31].

4.12. RNA isolation and quantitative RT-PCR

TRIzol Reagent (Invitrogen, Carlsbad, CA) was used to extract total RNA from the HCT116 cells after treatment with 5 μM, 10 μM, 20 μM **A23** according to the manufacturer's guidelines. Then using AMV reverse transcriptase (TaKaRa, Dalian, China) and oligo dT to reverse-transcribe total RNA (1 μg) to cDNA. The reaction conditions were as follows: 16 °C for 5 min, 42 °C for 60 min and 85 °C for 5 min. After that, real-time PCR was performed using SYBR Green Dye (Invitrogen, Carlsbad, CA) and specific primers including c-Caspase 3, c-Caspase4, c-Caspase 8, c-Caspase 9, Bcl-2, BAX, and GAPDH on a LightCycler® 480 II System (Roche). The reactions were incubated at 95 °C for 5 min, followed by 40 cycles of 95 °C for 30 s, 60 °C for 30 s and 72 °C for 30 s. The relative amount of target mRNA was normalized to GAPDH mRNA [33]. The gene expression was calculated using the $2^{-\triangle\triangle CT}$ equation, in which $\triangle\triangle C_T = (C_{T\ mRNA} - C_{T\ GAPDH})_{target} - (C_{T\ mRNA} - C_{T\ GAPDH})_{control}$. The PCR primers used here are given in Table S1.

4.13. Protein isolation and Western blotting

After treated with 5 μM, 10 μM, 20 μM **A23**, the HCT116 cells were lysed in RIPA lysis buffer (Beyotime, Shanghai, China) for 30 min on ice. Then centrifuged at 12,000*g* at 4 °C for 10 min and collected the supernatant. Using the BCA protein assay kit (Thermo Scientific, Rockford, IL, USA) to calculate the concentration of protein. Then, equivalent quantities of protein were separated by 10% SDS-PAGE (Bio-Rad). After electrophoresis, the proteins were transferred onto PVDF membranes (Millipore, Bedford, MA, USA). After that, blocking the PVDF membranes with 5% non-fat milk at room temperature for 1 h and immunostaining the PVDF membranes with the primary antibodies overnight at 4 °C. The next step is washing the PVDF membranes four times (once every quarter) in 1 × TBST, and then incubated with a secondary antibody at room temperature for 1 h. The signals of each band were detected with an enhanced chemiluminescence reagent (Thermo Scientific, Rockford, IL, USA). The protein levels were normalized by probing the same blots with a GAPDH antibody [34]. The antibodies were purchased from the following sources: anti-c-Caspase 6: (Cell Signaling Technology Inc., USA) , anti-c-Caspase 7: (Cell Signaling Technology Inc., USA), anti-c-Caspase 9: (Cell Signaling Technology Inc., USA), anti-AKT1(Cell Signaling Technology Inc., USA), anti-p-ERK1/2 (Cell Signaling Technology Inc., USA), anti-c-parp: (Cell Signaling Technology Inc., USA), and anti-GAPDH (Cell Signaling Technology Inc., USA). ImageJ software was used to quantify the protein levels.

Declaration of Competing Interest

The authors declare that they have no known competing financial interests or personal relationships that could have appeared to influence the work reported in this paper.

Acknowledgements

We would like to express our gratitude to our colleagues, Chen-Wen Shao and Kang-Min Zhou, for their help in the experiments.

Appendix A. Supplementary material

Supplementary data to this article can be found online at https://doi.org/10.1016/j.bioorg.2020.104390.

References

[1] A. Lisowski, M. Rell-Bakalarska, L. Rutkowska-Sak, The ups and downs of non-steroidal anti-inflammatory drugs, Reumatologia 44 (2006) 106–111.
[2] K. Tsuge, T. Inazumi, A. Shimamoto, Y. Sugimoto, Molecular mechanisms underlying prostaglandin E2-exacerbated inflammation and immune diseases, Int. Immunol. 31 (2019) 597–606.
[3] G.F. Meresman, C. Olivares, Involvement of prostaglandins in the pathophysiology of endometriosis, Basic Concepts Curr. Res. Trends Endometriosis (2012) 115–135.
[4] F. Cipollone, G. Cicolini, M. Bucci, Cyclooxygenase and prostaglandin synthases in atherosclerosis: recent insights and future perspectives, Pharmacol. Ther. 118 (2008) 161–180.
[5] S. Mehrotra, A. Morimiya, B. Agarwal, R. Konger, S. Badve, Microsomal prostaglandin E2 synthase-1 in breast cancer: a potential target for therapy, J. Pathol. 208 (2006) 356–363.
[6] C.H. Tsai, M.Y. Chou, Y.C. Chang, The up-regulation of cyclooxygenase-2 expression in human buccal mucosal fibroblasts by arecoline: a possible role in the pathogenesis of oral submucous fibrosis, J. Oral Pathol. Med.: Off. Publ. Int. Assoc. Oral Pathol. Am. Acad. Oral Pathol. 32 (2003) 146–153.
[7] A. Maitra, R. Ashfaq, C.R. Gunn, A. Rahman, C.J. Yeo, T.A. Sohn, J.L. Cameron, R. H. Hruban, R.E. Wilentz, Cyclooxygenase 2 expression in pancreatic adenocarcinoma and pancreatic intraepithelial neoplasia: an immunohistochemical analysis with automated cellular imaging, Am. J. Clin. Pathol. 118 (2002) 194–201.
[8] J.A. Glover, C.M. Hughes, M.M. Cantwell, L.J. Murray, A systematic review to establish the frequency of cyclooxygenase-2 expression in normal breast epithelium, ductal carcinoma in situ, microinvasive carcinoma of the breast and invasive breast cancer, Br. J. Cancer 105 (2011) 13–17.
[9] W.A. Ray, T.M. MacDonald, D.H. Solomon, D.J. Graham, J. Avorn, COX-2 selective non-steroidal anti-inflammatory drugs and cardiovascular disease, Pharmacoepidemiol. Drug Saf. 12 (2003) 67–70.
[10] S. Grosch, I. Tegeder, E. Niederberger, L. Brautigam, G. Geisslinger, COX-2 independent induction of cell cycle arrest and apoptosis in colon cancer cells by the selective COX-2 inhibitor celecoxib, FASEB J.: Off. Publ. Federat. Am. Soc. Exp. Biol. 15 (2001) 2742–2744.
[11] S. Kanaoka, T. Takai, K.I. Yoshida, Cyclooxygenase-2 and tumor biology, Adv. Clin. Chem. 43 (2007) 59–78.
[12] M.-E. St-Germain, V. Gagnon, I. Mathieu, S. Parent, E. Asselin, Akt regulates COX-2 mRNA and protein expression in mutated-PTEN human endometrial cancer cells, Int. J. Oncol. 24 (2004) 1311–1324.
[13] D. Morgensztern, H.L. McLeod, PI3K/Akt/mTOR pathway as a target for cancer therapy, Anticancer Drugs 16 (2005) 797–803.
[14] D.G. Binion, M.F. Otterson, P. Rafiee, Curcumin inhibits VEGF-mediated angiogenesis in human intestinal microvascular endothelial cells through COX-2 and MAPK inhibition, Gut 57 (2008) 1509–1517.
[15] D. Wang, P. Liu, Ingenol-3-angelate suppresses growth of melanoma cells and skin tumor development by downregulation of NF-kappaB-Cox2 signaling, Med. Sci. Monitor: Int. Med. J. Exp. Clin. Res. 24 (2018) 486–502.

[16] M. Zhu, Y. Zhu, P. Lance, TNFalpha-activated stromal COX-2 signalling promotes proliferative and invasive potential of colon cancer epithelial cells, Cell Prolif. 46 (2013) 374–381.
[17] J. Lee, H.H. Jung, Y.H. Im, J.H. Kim, J.O. Park, K. Kim, W.S. Kim, J.S. Ahn, C. W. Jung, Y.S. Park, W.K. Kang, K. Park, Interferon-alpha resistance can be reversed by inhibition of IFN-alpha-induced COX-2 expression potentially via STAT1 activation in A549 cells, Oncol. Rep. 15 (2006) 1541–1549.
[18] R. Kumar, A. Sharma, A. Kumari, A. Gulati, Y. Padwad, R. Sharma, Epigallocatechin gallate suppresses premature senescence of preadipocytes by inhibition of PI3K/Akt/mTOR pathway and induces senescent cell death by regulation of Bax/Bcl-2 pathway, Biogerontology 20 (2019) 171–189.
[19] N.K. Altorki, R.S. Keresztes, J.L. Port, D.M. Libby, R.J. Korst, D.B. Flieder, C. A. Ferrara, D.F. Yankelevitz, K. Subbaramaiah, M.W. Pasmantier, A.J. Dannenberg, Celecoxib, a selective cyclo-oxygenase-2 inhibitor, enhances the response to preoperative paclitaxel and carboplatin in early-stage non-small-cell lung cancer, J. Clin. Oncol.: Off. J. Am. Soc. Clin. Oncol. 21 (2003) 2645–2650.
[20] J. Li, H. Gao, S. Su, Y. Wang, Relationship between antitumor effect of valdecoxib and COX-2 expression, pp. 243–246.
[21] K.A.M. Abouzid, N.A. Khalil, E.M. Ahmed, H.A.A. El-Latif, M.E. El-Araby, Structure-based molecular design, synthesis, and in vivo anti-inflammatory activity of pyridazinone derivatives as nonclassic COX-2 inhibitors, Med. Chem. Res. 19 (2009) 629–642.
[22] P. Asadi, G. Khodarahmi, A. Jahanian-Najafabadi, L. Saghaie, F. Hassanzadeh, Synthesis, characterization, molecular docking studies and biological evaluation of some novel hybrids based on quinazolinone, benzofuran and imidazolium moieties as potential cytotoxic and antimicrobial agents, Iranian J. Basic Med. Sci. 20 (2017) 975–989.
[23] Q. Wang, M. Zhu, R. Zhu, L. Lu, C. Yuan, S. Xing, X. Fu, Y. Mei, Q. Hang, ChemInform abstract: exploration of α-aminophosphonate N-derivatives as novel, potent and selective inhibitors of protein tyrosine phosphatases, ChemInform 43 (2012).
[24] S.A. Dake, D.S. Raut, K.R. Kharat, R.S. Mhaske, S.U. Deshmukh, R.P. Pawar, Ionic liquid promoted synthesis, antibacterial and in vitro antiproliferative activity of novel α-aminophosphonate derivatives, Bioorg. Med. Chem. Lett. 21 (2011) 2527–2532.
[25] J.-Z. Liu, B.-A. Song, H.-T. Fan, P.S. Bhadury, W.-T. Wan, S. Yang, W. Xu, J. Wu, L.-H. Jin, X. Wei, D.-Y. Hu, S. Zeng, Synthesis and in vitro study of pseudo-peptide thioureas containing α-aminophosphonate moiety as potential antitumor agents, Eur. J. Med. Chem. 45 (2010) 5108–5112.
[26] X.C. Huang, M. Wang, Y.M. Pan, G.Y. Yao, H.S. Wang, X.Y. Tian, J.K. Qin, Y. Zhang, Synthesis and antitumor activities of novel thiourea α-aminophosphonates from dehydroabietic acid, Eur. J. Med. Chem. 69 (2013) 508–520.
[27] L. Jin, B. Zhang, S. Hua, M. Ji, X. Huang, R. Huang, H. Wang, Glycyrrhetinic acid derivatives containing aminophosphonate ester species as multidrug resistance reversers that block the NF-κB pathway and cell proliferation, Bioorg. Med. Chem. Lett. 28 (2018) 3700–3707.
[28] A. Mucha, P. Kafarski, Ł. Berlicki, Remarkable potential of the α-aminophosphonate/phosphinate structural motif in medicinal chemistry, J. Med. Chem. 54 (2011) 5955–5980.
[29] S. Sobhani, Z. Tashrifi, Al(OTf)3as an efficient catalyst for one-pot synthesis of primary diethyl 1-aminophosphonates under solvent-free conditions, Synth. Commun. 39 (2008) 120–131.
[30] Z. Li, Z.C. Wang, X. Li, M. Abbas, S.Y. Wu, S.Z. Ren, Q.X. Liu, Y. Liu, P.W. Chen, Y. T. Duan, P.C. Lv, H.L. Zhu, Design, synthesis and evaluation of novel diaryl-1,5-diazoles derivatives bearing morpholine as potent dual COX-2/5-LOX inhibitors and antitumor agents, Eur. J. Med. Chem. 169 (2019) 168–184.
[31] M.Y. Ye, G.Y. Yao, Y.M. Pan, Z.X. Liao, Y. Zhang, H.S. Wang, Synthesis and antitumor activities of novel alpha-aminophosphonate derivatives containing an alizarin moiety, Eur. J. Med. Chem. 83 (2014) 116–128.
[32] S.Z. Ren, Z.C. Wang, X.H. Zhu, D. Zhu, Z. Li, F.Q. Shen, Y.T. Duan, H. Cao, J. Zhao, H.L. Zhu, Design and biological evaluation of novel hybrids of 1, 5-diarylpyrazole and Chrysin for selective COX-2 inhibition, Bioorg. Med. Chem. 26 (2018) 4264–4275.
[33] Y. Liu, D. Li, Z. Liu, Y. Zhou, D. Chu, X. Li, X. Jiang, D. Hou, X. Chen, Y. Chen, Z. Yang, L. Jin, W. Jiang, C. Tian, G. Zhou, K. Zen, J. Zhang, Y. Zhang, J. Li, C. Y. Zhang, Targeted exosome-mediated delivery of opioid receptor Mu siRNA for the treatment of morphine relapse, Sci. Rep. 5 (2015) 17543.
[34] Y. Gu, S. Liu, X. Zhang, G. Chen, H. Liang, M. Yu, Z. Liao, Y. Zhou, C.Y. Zhang, T. Wang, C. Wang, J. Zhang, X. Chen, Oncogenic miR-19a and miR-19b co-regulate tumor suppressor MTUS1 to promote cell proliferation and migration in lung cancer, Protein Cell 8 (2017) 455–466.